On the internal structure of relativistic jets with zero velocity along the axis

V. S. Beskin,[1,2,3]⋆ F. A. Kniazev[2] and K. Chatterjee [4,5]

[1]*P.N.Lebedev Physical Institute, Leninsky prospekt 53, Moscow 119991, Russia*
[2]*Moscow Institute of Physics and Technology (State Research University), Institutsky per. 9, Dolgoprudny 141700, Russia*
[3]*National Research Center 'Kurchatov Institute', Kurchatov sqr. 1, Moscow 123182, Russia*
[4]*Black Hole Initiative at Harvard University, 20 Garden Street, Cambridge, MA 02138, USA*
[5]*Harvard-Smithsonian Center for Astrophysics, 60 Garden Street, Cambridge, MA 02138, USA*

ABSTRACT

The present work is devoted to the analysis of the internal structure of relativistic jets under the condition that the velocity of the plasma flow at the jet axis vanishes. It is shown that in spite of the seemingly fundamental difference in the formulation of the problem at the axis, the key properties of the internal structure of such relativistic jets remain the same as for non-zero velocity along the axis. In both cases, at a sufficiently low ambient pressure, a dense core appears near the axis, the radius of which is close to the size of the light cylinder.

Key words: galaxies: active – galaxies: jets.

1 INTRODUCTION

The significant progress of radio interferometry at long baselines makes it possible to directly explore the internal structure of relativistic jets from active galactic nuclei (AGN; Gabuzda, Murray & Cronin 2004; Kovalev et al. 2007; Hovatta et al. 2012; Lister et al. 2016; Mertens et al. 2016; Hodge et al. 2018; Zobnina et al. 2022), which are visible manifestations of their activity at an early stage of evolution (Begelman, Blandford & Rees 1984; Urry & Padovani 1995; Davis & Tchekhovskoy 2020; Komissarov & Porth 2021). Such detailed observational studies allow us to test the numerous predictions of the theory of strongly magnetized outflows that have been developed since the 1970s (Blandford 1976; Lovelace 1976; Camenzind 1986; Heyvaerts & Norman 1989; Camenzind 1990; Takahashi et al. 1990; Chiueh, Li & Begelman 1991; Appl & Camenzind 1992; Bogovalov 1992; Pelletier & Pudritz 1992; Beskin & Pariev 1993; Eichler 1993; Lery et al. 1999; Beskin & Malyshkin 2000; Beskin & Nokhrina 2006, 2009; Lyubarsky 2009). The main conclusions of these theoretical papers, discussed in several reviews and monographs (Begelman et al. 1984; Heyvaerts 1996; Krolik 1999; Camenzind 2007; Beskin 2010; Meier 2012), were later confirmed by numerical simulations of jets from accreting black holes (Ustyugova et al. 1995, 1999; McKinney 2006; Komissarov et al. 2007; Tchekhovskoy, McKinney & Narayan 2008; Romanova et al. 2009; Porth et al. 2011; McKinney, Tchekhovskoy & Blandford 2012; Chatterjee et al. 2019).

One of these theoretical predictions repeatedly confirmed by numerical simulations is the existence of a universal asymptotic behaviour for the Lorentz factor of an outflow $\gamma = \varpi/R_L$, where ϖ is the distance from the rotation axis, and $R_L = c/\Omega$ is the radius of the light cylinder (Ω is the angular velocity of the central engine). As another example, one can mention the presence of a central dense

cylindrical core with the radius

$$r_{\rm core} = u_{\rm in} R_L, \tag{1}$$

where $u_{\rm in}$ is the four-velocity of a flow along rotation axis. This result was first obtained analytically (Chiueh et al. 1991; Eichler 1993; Bogovalov 1995, 1998; Beskin & Malyshkin 2000; Beskin & Nokhrina 2006, 2009; Lyubarsky 2009) and later confirmed numerically (Komissarov et al. 2007; Tchekhovskoy et al. 2008; Porth et al. 2011). As shown in Fig. 1, this core is formed over long enough distances $z > z_{\rm cr}$ from the central engine when the transverse dimension of the jet $r_{\rm jet}$ becomes larger than $r_{\rm cr} = (u_{\rm in}\sigma_M)^{1/2}R_L$. Accordingly, the poloidal magnetic field at this distance $B_{\rm cr} = B_p(z_{\rm cr})$ becomes equal to

$$B_{\rm cr} = \frac{B_L}{\sigma_M u_{\rm in}}. \tag{2}$$

Here, σ_M is the Michel magnetization parameter and B_L is the magnetic field on the light cylinder near the origin (see formal definitions below). It is necessary to emphasize that relation (1) was also verified for non-relativistic flows, i.e. for $u_{\rm in} \ll 1$ (Bogovalov & Tsinganos 1999; Lery et al. 1999; Tsinganos & Bogovalov 2002; Beskin & Nokhrina 2009).

We emphasize that, as was already known in the late 1990s, the internal structure of relativistic jets is very sensitive to the behaviour of the solution of the Grad–Shafranov (GS) equation near the axis (Chiueh et al. 1991; Eichler 1993; Bogovalov 1995; Lyubarskii 1997). The difficulty of solving the GS equation in this region proved to be the stumbling block that did not allow us to link together the various asymptotic solutions obtained. Only after the work by Beskin & Malyshkin (2000) did it become clear that the central core exists only for sufficiently low ambient medium pressure $P_{\rm ext} < P_{\rm cr}$ (i.e. at sufficiently large distances from the central engine), where $P_{\rm cr} = B_{\rm cr}^2/8\pi$. For larger ambient pressures $P_{\rm ext} > P_{\rm cr}$ (i.e. at small distances $z < z_{\rm cr}$), the poloidal magnetic field remains practically constant within the whole jet.

⋆ E-mail: beskin@lpi.ru
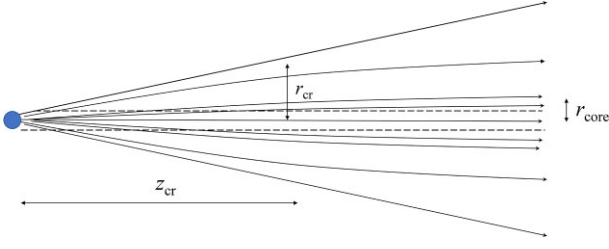
Figure 1. The structure of the magnetic field in the model under consideration. At a distances $z > z_{cr}$ from the central engine, when the transverse size of the jet reaches the scale $\sim r_{cr}$, in a conical flow (in which the plasma density and the magnetic field weakly depend on the distance from the axis), a denser central core begins to form. The light cylinder is shown by a dashed line.

As a result, depending on the ambient pressure $P_{ext} < P_{cr}$, the poloidal magnetic field B_p outside the central core has the form

$$B_p \propto \varpi^{-\alpha} \tag{3}$$

with $0 < \alpha < 1$. At the same time, however, the magnetic field in the core itself does not differ significantly from the value B_{cr}. In this case, the jet remains magnetically dominated till the distance from the origin when the external pressure drops to $P_{ext} \approx P_{eq} = B_{eq}^2/8\pi$, where $B_{eq} = \sigma_M^{-2} B_L$. At lower ambient pressures, the flow becomes particle-dominated.

Here, however, one important remark should be made. This model explicitly assumed that the flow velocity along the jet axis itself does not vanish. In fact, relation (1) that, in the non-relativistic regime (i.e. $u_{in} \to 0$), the core radius $r_{core} \to 0$ as well. Thus, in the non-relativistic regime, $r_{core} \to 0$ when u_{in} tends to zero. Thus, the very existence of the central core is called into question. Whether this result remains valid if the flow velocity vanishes on the jet axis has not been considered in detail up to now.

It must be said that the very assumption that the velocity on the jet axis is not equal to zero still had some grounds. It is based on the model of plasma generation in the vacuum region near the black hole surface (Beskin, Istomin & Parev 1992; Hirotani & Okamoto 1998; Ptitsyna & Neronov 2016; Crinquand et al. 2020), which is equivalent to the so-called 'outer gap' in the magnetosphere of radio pulsars. In this case, the value u_{in} arises as a natural boundary condition for the GS equation (Beskin & Kuznetsova 2000), which ultimately leads to the existence of a central core.

On the other hand, there is also support for outflow models with zero velocity along the jet axis. For example, this occurs when the only mechanism of plasma acceleration is via electromagnetic forces (the Poynting vector flux on the jet axis is equal to zero). This point of view can also be supported by the pioneering work of Takahashi et al. (1990), who introduced the notion of a stagnation point, i.e. the region of the base of the flow where the velocity is zero. It was further shown that the hydrodynamical motion in a strongly magnetized flow is completely determined by the electric drift; the motion along the magnetic field lines can be neglected (Tchekhovskoy et al. 2008; Beskin 2010). Despite the fact that this result concerns only the asymptotically far region $\varpi \gg R_L$, it began to be used inside the light cylinder as well (see e.g. Takahashi et al. 2018). Finally, the zero velocity along the jet axis was reproduced in recent numerical simulation (Chatterjee et al. 2019).

As was already emphasized, since the results of (1)–(2) discussed above were obtained under the assumption of a non-zero velocity along the jet axis, it is important to discuss the question of whether such an internal structure of relativistic jets is preserved under the

assumption $u_{in}(0) = 0$. The present work is devoted precisely to this issue. As will be shown, the seemingly fundamental difference in the formulation of the problem does not change the key properties of the internal structure of relativistic jets. Moreover, relations $r_{core} \approx R_L$ and $B_{cr} \approx \sigma_M^{-1} B_L$ also remain valid.

The paper is organized as follows. In Section 2, we formulate the basic equation describing cylindrical cold magnetized flow. Section 3 is devoted to the analysis of singular points. In the problem considered here, this is the rotation axis, as well as the Alfvénic surface near the light cylinder. Finally, in Section 4, we formulate the main results of our consideration.

2 BASIC EQUATIONS

Below we use the language developed by Thorne, Price & MacDonald (1986): all 3D vectors correspond to physical quantities measured by Zero Angular Momentum Observers (which in our case, i.e. far from the central black hole, coincides with the usual cylindrical reference frame). Further, it should be immediately noted that our task is not devoted to the construction of a global solution. It is dedicated to the area far beyond the plasma generation region. Therefore, the region of plasma generation participates in our analysis indirectly through the integrals of motion, which we will try to choose in the most reasonable way.

Besides, as was shown by Beskin & Nokhrina (2006), one can consider strongly collimated jet as a sequence of cylindrical flows. This makes it possible to explore their internal structure by analysing not the second-order GS equation, but two first-order ordinary differential equations for magnetic flux $\Psi(\varpi)$ and poloidal Alfvénic Mach number $\mathcal{M}(\varpi)$ (Beskin 1997; Beskin & Malyshkin 2000)

$$\mathcal{M}^2 = \frac{4\pi\mu\eta^2}{n}. \tag{4}$$

Here, n is the number density in the comoving reference frame and μ is relativistic enthalpy. Accordingly, η is the particle-to-magnetic flux ratio determined from relation

$$n\boldsymbol{u}_p = \eta\boldsymbol{B}_p, \tag{5}$$

which is constant along magnetic field lines: $\eta = \eta(\Psi)$. Finally, by definition, in the cylindrical geometry

$$B_z = \frac{1}{2\pi\varpi}\frac{d\Psi}{d\varpi}, \tag{6}$$

$$B_\varphi = -\frac{2I}{c\varpi}.$$

Here, I is the total electric current flowing within the magnetic tube $\Psi = $ const.

The first equation is the relativistic Bernoulli equation

$$u_p^2 = \gamma^2 - u_\varphi^2 - 1, \tag{7}$$

where u_p and u_φ are the poloidal and toroidal components of the 4-velocity $\boldsymbol{u}$, respectively. It can be rewritten in the form (Beskin 2010)

$$\frac{\mathcal{M}^4}{64\pi^4\varpi^2}\left(\frac{d\Psi}{d\varpi}\right)^2 = \frac{K}{\varpi^2 A^2} - \mu^2\eta^2. \tag{8}$$

Here,

$$A = 1 - \Omega_F^2\varpi^2/c^2 - \mathcal{M}^2 \tag{9}$$

is the Alfvénic factor, where the so-called field angular velocity $\Omega_F = \Omega_F(\Psi)$ is constant on the magnetic surfaces ($\Omega_F = \Omega$ near the central

engine),

$$K = \varpi^2 (e')^2 (A - \mathcal{M}^2) + \mathcal{M}^4 \varpi^2 E^2 - \mathcal{M}^4 L^2 c^2, \tag{10}$$

and by definition,

$$e'(\Psi) = E(\Psi) - \Omega_F(\Psi) L(\Psi). \tag{11}$$

Remember that Bernoulli integral $E = E(\Psi)$ and the angular momentum flux $L = L(\Psi)$

$$E(\Psi) = \gamma \mu \eta c^2 + \frac{\Omega_F I}{2\pi}, \tag{12}$$

$$L(\Psi) = \varpi u_\varphi \mu \eta c + \frac{I}{2\pi}, \tag{13}$$

together with the angular velocity $\Omega_F(\Psi)$ are also integrals of motion. In this case, the current I, the Lorentz factor γ, and the toroidal four-velocity u_φ are expressed as follows

$$\frac{I}{2\pi} = \frac{L - \Omega_F \varpi^2 E / c^2}{1 - \Omega_F^2 \varpi^2 / c^2 - \mathcal{M}^2}, \tag{14}$$

$$\gamma = \frac{1}{\mu\eta} \frac{(E - \Omega_F L) - E \mathcal{M}^2}{1 - \Omega_F^2 r^2 / c^2 - \mathcal{M}^2}, \tag{15}$$

$$u_\varphi = \frac{1}{\mu\eta c \varpi} \frac{(E - \Omega_F L) \Omega_F \varpi^2 / c^2 - L \mathcal{M}^2}{1 - \Omega_F^2 r^2 / c^2 - \mathcal{M}^2}. \tag{16}$$

The second equation determines the Mach number $\mathcal{M}$ for a cold flow (the sound speed $c_s = 0$ and the relativistic enthalpy $\mu = m_p c^2 = $ const) and is given by (Beskin 2010):

$$\left[\frac{(e')^2}{\mu^2\eta^2 c^4} - 1 + \frac{\Omega_F^2 \varpi^2}{c^2} \right] \frac{d\mathcal{M}^2}{d\varpi} = \frac{\mathcal{M}^6 L^2}{A \varpi^3 \mu^2 \eta^2 c^2}$$
$$+ \frac{\Omega_F^2 \varpi \mathcal{M}^2}{c^2} \left[2 - \frac{(e')^2}{A \mu^2 \eta^2 c^4} \right] + \mathcal{M}^2 \frac{e'}{\mu^2 \eta^2 c^4} \frac{d\Psi}{d\varpi} \frac{de'}{d\Psi}$$
$$+ \frac{\mathcal{M}^2 \varpi^2}{2c^2} \frac{d\Psi}{d\varpi} \frac{d\Omega_F^2}{d\Psi} - \mathcal{M}^2 \left(1 - \frac{\Omega_F^2 \varpi^2}{c^2} \right) \frac{d\Psi}{d\varpi} \frac{1}{\eta} \frac{d\eta}{d\Psi}. \tag{17}$$

Let us now define the integrals of motion in a convenient form. In contrast to the basic assumption on the finite velocity along the jet axis discussed earlier, we must now, following (5), set $\eta(\Psi) \to 0$ as $\Psi \to 0$. At the same time, thanks to the definitions (12)–(13), it is convenient to express the invariant $e'(\Psi)$ (11) in terms of the flux ratio $\eta(\Psi)$ and an additional function $\varepsilon(\Psi)$

$$(e')^2 = \mu^2 \eta^2(\Psi) c^4 - \mu^2 \eta^2(\Psi) c^4 \varepsilon(\Psi). \tag{18}$$

As can be seen from relations (12)–(13), the value of ε vanishes for zero flow velocity. Therefore, it turns out to be convenient in the analysis of the problem under consideration. In particular, the function $\varepsilon(\Psi)$ cannot have an arbitrary form. We clarify this issue a little later.

Besides, following (Beskin et al. 2017; Chernoglazov, Beskin & Pariev 2019), we set

$$L(\Psi) = \frac{\Omega_0 \Psi}{4\pi^2} \sqrt{1 - \frac{\Psi}{\Psi_{tot}}}, \tag{19}$$

$$\Omega_F(\Psi) = \Omega_0 \sqrt{1 - \frac{\Psi}{\Psi_{tot}}}. \tag{20}$$

Such definitions ensure the closure of the longitudinal electric current within the jet. Further, thanks to (11) and (18), we have

$$E(\Psi) = \Omega_F(\Psi) L(\Psi) + \mu \eta(\Psi) c^2 [1 - \varepsilon(\Psi)]^{1/2}. \tag{21}$$

Finally, due to our main assumption $\eta(0) = 0$, the fourth integral $\eta(\Psi)$, in the limit $\Psi \to 0$, can be written as

$$\eta(\Psi) = \eta_0 \left(\frac{\Psi}{\Psi_{tot}} \right)^\beta, \tag{22}$$

where $\beta > 0$. Below, for simplicity, we assume that the relation (22) is valid for any value of Ψ.

Introducing the dimensionless variables

$$x = \frac{\Omega_0 \varpi}{c}, \tag{23}$$

$$y = \frac{\Psi}{\Psi_{tot}}, \tag{24}$$

one can rewrite equations (8) and (17) as

$$\frac{dy}{dx} = \frac{\eta(y)x}{\sigma_M |A| \mathcal{M}^2} \Big[f(x, y)[1 - \omega^2(y)x^2 - 2\mathcal{M}^2]$$
$$- \mathcal{M}^4 \varepsilon(y) + 4\sigma_M \mathcal{M}^4 \frac{\omega(y) l(y)}{\eta(y)} [1 - \varepsilon(y)]^{1/2}$$
$$+ 4\sigma_M^2 \mathcal{M}^4 [\omega^2(y)x^2 - 1] \frac{l^2(y)}{x^2 \eta^2(y)} \Big]^{1/2}, \tag{25}$$

$$\frac{f(x, y)}{\mathcal{M}^2} \frac{d\mathcal{M}^2}{dx} = 4\sigma_M^2 \frac{\mathcal{M}^4}{Ax^3} \frac{l^2(y)}{\eta^2(y)} + x\omega^2(y)$$
$$- \frac{x\omega^2(y)}{A} \Big[f(x, y) + \mathcal{M}^2 \Big] - \frac{1}{2} \frac{d\varepsilon(y)}{dy} \frac{dy}{dx}$$
$$+ \frac{1}{2} x^2 \frac{d\omega^2(y)}{dy} \frac{dy}{dx} + \frac{1}{2} \frac{f(x, y)}{\eta^2(y)} \frac{d\eta^2(y)}{dy} \frac{dy}{dx}. \tag{26}$$

Here,

$$\sigma_M = \frac{\Omega_0^2 \Psi_{tot}}{8\pi^2 \mu \eta_0 c^2} \tag{27}$$

is the Michel magnetization parameter already mentioned above, $\eta(\Psi) = \eta_0 \eta(y)$, and now

$$A = 1 - \omega^2(y)x^2 - \mathcal{M}^2. \tag{28}$$

Further, we introduce new important function

$$f(x, y) = \omega^2(y)x^2 - \varepsilon(y). \tag{29}$$

Finally, despite the fact that according to (19), (20), and (22), we have $l(y) = y(1 - y)^{1/2}$, $\omega(y) = (1 - y)^{1/2}$, and $\eta(y) = y^\beta$, we have kept their literal expressions in equations (25) and (26).

3 SINGULAR POINTS

3.1 Rotation axis

Before integrating equations (25)–(26), let us discuss their behaviour for $x \to 0$. This helps us with numerical integration as well. Below we assume that poloidal magnetic field B_z and the number density n are finite at the rotation axis. Then, due to definition (4), $\mathcal{M}^2 \to 0$ if $\eta \to 0$. Storing now only the leading terms (and grouping the similar ones), we obtain

$$\frac{dy}{dx} = \frac{\eta(y)x}{\sigma_M \mathcal{M}^2} f^{1/2}, \tag{30}$$

$$\frac{f^{3/2} \eta(y)}{\mathcal{M}^2} \frac{d}{dx} \left[\frac{\mathcal{M}^2}{f^{1/2} \eta(y)} \right] + (f + \mathcal{M}^2)x = 4\sigma_M^2 \frac{\mathcal{M}^4 y^2}{x^3 \eta^2(y)}. \tag{31}$$

As one can see, the function $f(x, y)$ plays the primary role in determining the behaviour of the solution near the rotation axis, and thus, the function $\varepsilon(y)$ should be introduced. In order to understand the functional form of $\varepsilon(y)$ for our problem statement, let us suppose that the magnetic field is regular at $x \to 0$. In this case, it is convenient to introduce the dimensionless magnetic field

$$b = \frac{B_z}{B_L}, \tag{32}$$

where B_L is the magnetic field on the light cylinder near the origin and can be determined from the condition $\Psi_{tot} = \pi R_L^2 B_L$. It gives

$$b(x) = \frac{1}{2x} \frac{dy}{dx}. \tag{33}$$

In particular, denoting $b_0 = b(0)$, we get for $x \to 0$

$$y(x) \approx b_0 x^2. \tag{34}$$

In what follows, we will be interested in the case $b_0 \ll 1$, because the light cylinder must contain only a small part of the total magnetic flux as the size of the jet is much larger than the light cylinder.

Further, according to (12)–(13), we have for $v \ll c$,

$$\frac{e'(\Psi)}{\mu \eta(\Psi) c^2} = \gamma - \frac{\Omega_F \varpi}{c} u_\varphi = 1 + \frac{1}{2} \frac{v_p^2}{c^2} + \frac{1}{2} \frac{v_\varphi^2}{c^2} - \frac{\Omega_F \varpi}{c} \frac{v_\varphi}{c}. \tag{35}$$

Comparing this expression with the definition (18), we obtain

$$\varepsilon(y) = 2 \frac{\Omega_F \varpi}{c} \frac{v_\varphi}{c} - \frac{v_p^2}{c^2} - \frac{v_\varphi^2}{c^2}, \tag{36}$$

and thus, according to (29), we have

$$f(x, y) = \frac{(v_\varphi - \Omega_F \varpi)^2}{c^2} + \frac{v_p^2}{c^2}. \tag{37}$$

However, as is well known (see, e.g. Beskin 2010), relation (16) gives $v_\varphi \to \Omega_F \varpi$ for $\varpi \to 0$. Thus, $f(x, y) \to v_p^2/c^2$ as $x \to 0$. Using now definitions (4) and (5), we return to relation (30).

This result is certainly an important confirmation of the consistency of our approach. Moreover, it allows us to use relation (29) as a definition of $\varepsilon(y)$ for $y \to 0$. Together with (30), it gives

$$\varepsilon(y) = \frac{y}{b_0} - 4\eta^2(y) b_0^2 \mathcal{M}_0^4 \sigma_M^2. \tag{38}$$

Here, we introduce one more parameter

$$\mathcal{M}_0^2 = \frac{4\pi \mu \eta_0^2}{n_0}, \tag{39}$$

specifying the particle number density on the rotation axis $n_0 = n(0)$.

Relation (38) immediately allows us to make two important conclusions. Indeed, since $\varepsilon(y)$ is only a function of y, it cannot depend on such parameters as the magnetic field b_0 and the number density n_0 on any particular slice. This becomes possible only if the conditions

$$\eta(y) = y^{1/2} \tag{40}$$

and

$$\frac{1}{b_0} - 4 b_0^2 \mathcal{M}_0^4 \sigma_M^2 = \mathcal{C}, \tag{41}$$

where $\mathcal{C} = \text{const}$, are met. The first of them fixes the behaviour of the function $\eta(y)$ for $y \to 0$. As was already stressed, in what follows we assume that condition (40) is valid for all values of y. As for relation (41), we must now consider it as a connection between the magnetic field b_0 and the number density n_0 on the jet axis. Further, for estimates we can set $\mathcal{C} = 0$, so that $2 b_0 \mathcal{M}_0^2 \sigma_M \approx b_0^{-1/2} \gg 1$.
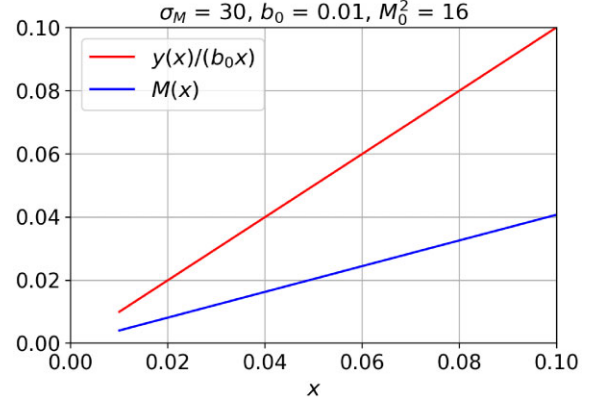
Returning now to equations (30)–(31) in the limit $x \to 0$, let us rewrite them in the form

$$\tilde{\beta}(x) = \frac{1}{2 b_0 \sigma_M} \frac{\eta(y) f^{1/2}}{\mathcal{M}^2(x)}, \tag{42}$$

$$-\frac{1}{\tilde{\beta}(x)} \frac{d\tilde{\beta}(x)}{dx} + \left(1 + \frac{\zeta}{\tilde{\beta}^2(x)}\right) x = \frac{x}{\tilde{\beta}^2(x)}. \tag{43}$$

Here,

$$\zeta = \frac{1}{4 b_0^2 \mathcal{M}_0^2 \sigma_M^2} = \frac{4\pi \mu n_0}{B_0^2} \ll 1, \tag{44}$$

Figure 2. Change in $y(x)/(b_0 x)$ and $\mathcal{M}(x)$ for small x, obtained as a solution of exact equations (25)–(26) using boundary conditions $y(x_0) = b_0 x_0^2$ and $\mathcal{M}^2(x_0) = x_0^2$ for $x_0 = 0.01$.

and $\tilde{\beta}(x) = b(x)/b_0$ so that $\beta(0) = 1$. As one can see, equation (43) is regular at $x \to 0$. It describes the change of the magnetic field. Actually, it depends on only one parameter ζ (44), which is small due to condition $b_0 \ll 1$. This confirms our assumption that the magnetic field remains finite at $x \to 0$.

As for equation (42), it can be now used to determine $\mathcal{M}^2(x)$ in the limit $x \to 0$. It finally gives

$$\mathcal{M}^2(x) \approx b_0 \mathcal{M}_0^2 x^2. \tag{45}$$

In Fig. 2, we show the change in $y(x)/(b_0 x) \approx x$ and $\mathcal{M}(x) \propto x$ for small x, obtained as an exact solution of equations (25)–(26) using boundary conditions $y(x_0) = b_0 x_0^2$ and $\mathcal{M}^2(x_0) = b_0 \mathcal{M}_0^2 x_0^2$ for $x_0 = 0.01$. As one can see, the exact solution is in full agreement with the analytical estimates (34) and (45).

3.2 Alfvénic surface

Before proceeding to a discussion of the general structure of a poloidal magnetic field outside the light cylinder, it is necessary to discuss the critical conditions on the Alfvénic surface $A = 0$. As for the fast magnetosonic surface, there is no singularity on it in the cylindrical geometry considered here (Beskin 2010). This well known effect is similar to the shift of the singularity into the modified fast magnetosonic surface in the self-similar Blandford & Payne (1982) solution. For cylindrical geometry, this singularity shifts to infinity.

As for the critical condition on the Alfvénic surface, it is more convenient to find it from the numerator of relation (15):

$$e'(\Psi_A) = E(\Psi_A) \mathcal{M}^2(r_A). \tag{46}$$

Here, all the quantities are to be taken at the Alfvénic point, so that $\Psi_A = \Psi(r_A)$. It is easy to check that, in this case, the regularity conditions in relations (14) and (16), as well as in our basic equations (25)–(26), are automatically fulfilled.

Note now that for the strongly magnetized flow ($\mathcal{M}^2 \ll 1$) under discussion, the Alfvénic surface is located near the light cylinder: $r_A \approx R_L$ (i.e. $x_A \approx 1$). Using the dimensionless variables (23)–(24) introduced above, one can rewrite the critical condition (46) as

$$2 \sigma_M \mathcal{M}_0^2 y \eta(y) = 1. \tag{47}$$

Taking into account relations (34) and (40) as well as under condition $x_A \approx 1$, we finally obtain

$$4 \sigma_M^2 \mathcal{M}_0^4 \approx b_0^{-3}. \tag{48}$$
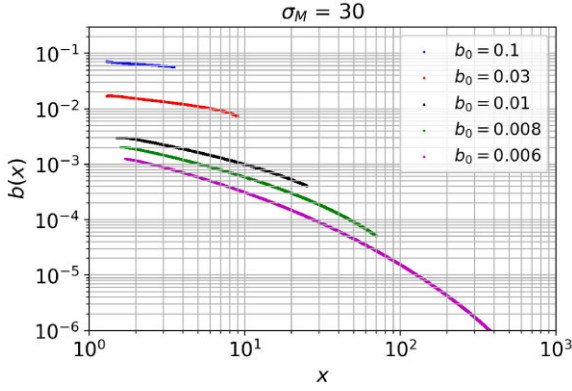
Figure 3. Dimensionless magnetic field $b(x)$ obtained from solutions of general equations (25)–(26). The jet size $x_{\mathrm{jet}} = r_{\mathrm{jet}}/R_{\mathrm{L}}$ is determined from the condition $\Psi(r_{\mathrm{jet}}) = \Psi_{\mathrm{tot}}$.

As we see, condition (48) is in accordance with relation (41) for $\mathcal{C} \approx 0$. Therefore, we will not dwell on the problem of passing the critical surface in detail and will immediately proceed to the analysis of the solution for $r > R_{\mathrm{L}}$ (or $x > 1$).

4 DISCUSSION AND CONCLUSION

In Fig. 3, we show solutions of general equations (25)–(26) for dimensionless magnetic field $b(x)$. We carry out the integration from the region of a singular point with boundary conditions corresponding to the asymptotic solutions (34) and (45) for $x = 1$. For this reason, the main control parameter is the magnetic field b_0 on the jet axis. The jet size r_{jet} is determined from the condition $\Psi(r_{\mathrm{jet}}) = \Psi_{\mathrm{tot}}$.

As one can see, despite the fact that the velocity at the axis vanishes, in general, there is complete qualitative agreement with the results obtained under the assumption of a finite flow velocity near the axis (see, e.g. Beskin & Nokhrina 2009; Lyubarsky 2009). The poloidal magnetic field B_z remains practically constant within the light cylinder. As for the structure of the magnetic field outside the light cylinder, it depends on the magnetic field b_0 on the jet axis. For sufficiently large values of b_0, longitudinal magnetic field remains essentially uniform ($B_z \approx \mathrm{const}$). But for small values of b_0, a central core begins to form near the jet axis, the size of which, however, does not tend to zero, as might be expected according to (1). In all cases, its size remains on the order of the radius of the light cylinder:

$$r_{\mathrm{core}} \approx R_{\mathrm{L}}. \qquad (49)$$

Additionally, there is a quantitative agreement if the expression (2) is corrected to

$$B_{\mathrm{cr}} \approx \frac{B_{\mathrm{L}}}{\sigma_{\mathrm{M}}}. \qquad (50)$$

For $\sigma_{\mathrm{M}} = 30$ shown in Fig. 3, expression (50) results in $b_0 = 0.03$ for the critical magnetic field. As one can see, this is exactly what takes place. Finally, as shown in Fig. 4, the universal asymptotic behaviour $\gamma \approx x$ is also reproduced with good accuracy outside the light cylinder.

On the other hand, we found one significant difference between the commonly assumed case $\eta(y) \approx \mathrm{const}$ and the case $\eta(y) = y^{1/2}$ considered in this paper. As shown in Fig. 5, particle number density $n_{\mathrm{lab}} = n\gamma$ in the laboratory reference frame remains almost constant outside the central core. This difference, however, can easily be explained.
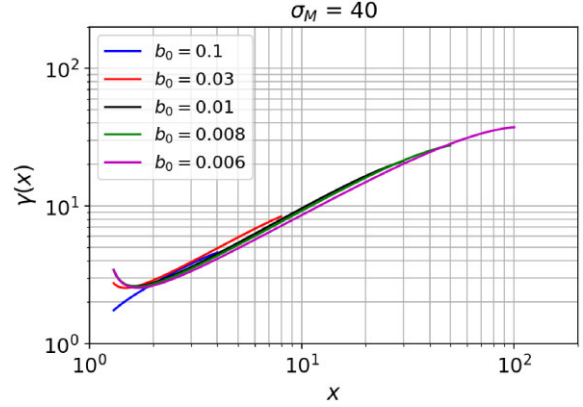
Figure 4. Lorentz-factor of particles $\gamma(x)$ as a function of distance from the axis x at different distances from "the central engine" outside the light cylinder. The downward bend at large x is associated with a rather small value of σ_{M}, which determines the maximum possible value of γ.
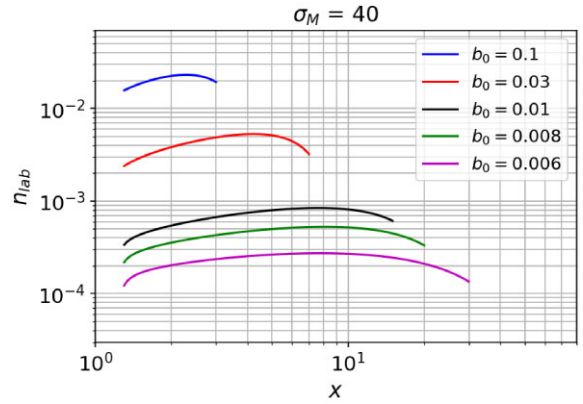
Figure 5. Particle number density $n_{\mathrm{lab}} = n\gamma$ in the laboratory reference frame as a function of distance from the axis x at different distances from "the central engine" outside the light cylinder.

Indeed, according to definition (4), the number density in the comoving reference frame can be written as $n = 4\pi\mu\eta^2/\mathcal{M}^2$. Further, far from the light cylinder ($\Omega_{\mathrm{F}}^2\varpi^2/c^2 \gg 1$), but in the region of a strongly magnetized flow ($\mathcal{M}^2 \ll \Omega_{\mathrm{F}}^2\varpi^2/c^2$), Lorentz factor γ according to (15) has the form

$$\gamma \approx \frac{\mathcal{M}^2 E c^2}{\mu\eta\Omega_{\mathrm{F}}^2\varpi^2}. \qquad (51)$$

Using now relations (19)–(21) to determine Bernoully integral E, we finally obtain

$$n_{\mathrm{lab}} \approx \frac{\eta\Psi}{\pi\varpi^2}. \qquad (52)$$

As a result, at a constant η and in the region of existence of the central core, when magnetic flux Ψ grows slowly than ϖ^2, the number density n_{lab} is to decrease with increasing distance ϖ from the axis. On the other hand, in the case $\eta = y^{1/2}$, depending on the behaviour of the solution $\Psi = \Psi(x)$, both an increase and a decrease in the number density n_{lab} with distance x from the axis are possible. Here, however, it should be noted that such behaviour takes place only if the relation $\eta = y^{1/2}$ remains valid up to the jet boundary. If this dependence takes place only at $x \to 0$ and at $x \sim 1$, we have $\eta \approx \mathrm{const}$, then the number density n_{lab} is to decrease with the distance from the axis.
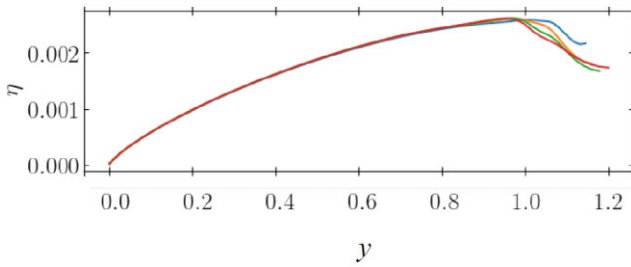
Figure 6. Function $\eta(y)$ reproduced from the results of a numerical simulation carried out by Chatterjee et al. (2019). Different curves correspond to different distances from "the central engine", confirming that $\eta(y)$ is indeed an integral of motion.
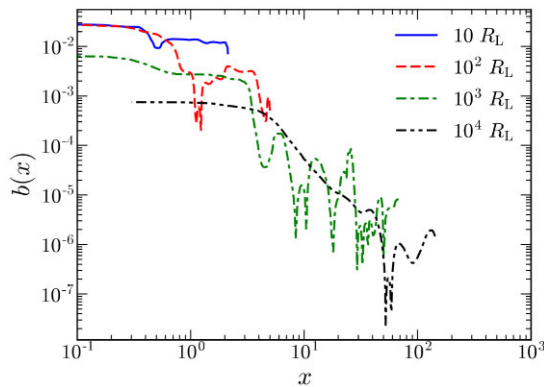
Figure 7. Dependence of the dimensionless poloidal magnetic field $b(x)$ on the distance to the axis $x = \varpi/R_L$ at different distances from the origin obtained by numerical simulation carried out by Chatterjee et al. (2019). The non-uniform behaviour of $b(x)$ at large x occurs to the jet boundary instabilities.

Moreover, our analytical results are in excellent agreement with the above-mentioned results of the numerical simulations of Chatterjee et al. (2019). First, Fig. 6 shows that jets in numerical simulations exhibit the dependence $\eta(y) \propto y^{1/2}$ (40), surprisingly matching the relation (40). Here, different curves correspond to different distances from "the central engine", confirming that $\eta(y)$ is indeed an integral of motion. We emphasize that the value of the integral $\eta(\Psi)$, like all other integrals of motion, was not set initially, as is done in analytical calculations, but emerged self-consistently as a result of evolving a time-dependent numerical simulation. Second, as shown in Fig. 7, the dependence of the dimensionless poloidal magnetic field $b(x)$ on the dimensionless distance to the axis $x = \varpi/R_L$ at different distances from the origin in the simulation also well reproduces the structure of the poloidal field shown in Fig. 3. As far as the number density distribution is concerned, it is determined by the magnetic field strength in the form of the so-called density floors (Porth et al. 2019), which does not allow us to determine it with sufficient accuracy. Therefore, we do not present here the results of the numerical simulation concerning the quantity n_{lab}.

Thus, we can state with confidence that the appearance of a central core at sufficiently large distances from the central engine does not depend on the plasma flow velocity near the jet axis. In all cases, at a sufficiently low ambient pressure, a dense core appears near the axis, the radius of which is close to the size of the light cylinder. Outside the central core, both the poloidal magnetic field and the plasma number density decrease with a power-law behaviour.

Finally, our results hold important implications for the jet structure and velocities at distances far from the black hole, relevant for interpreting observed jet morphologies and widths as well as the transverse jet velocity stratification measured in AGN jets (as was seen by Mertens et al. 2016; Park et al. 2019, for the M87 jet). Indeed, the presence of a central core region and a low-velocity region at the jet axis was also seen in global semianalytical work (Pu & Takahashi 2020; Takahashi, Kino & Pu 2021). As we show, once the central core forms at distances $z > z_{cr}$ from the black hole, the poloidal magnetic field in the jet becomes of the order of B_{cr}, the jet becomes susceptible to magnetic pinch and kink instabilities. This result is verified in 2D and 3D numerical simulations (Bromberg & Tchekhovskoy 2016; Chatterjee et al. 2019). Thus, we suggest that when a central core appears, the observed width of the jet will be determined precisely by the magnetically dominated inner jet region and not by the geometric width of the jet.

DATA AVAILABILITY

The data underlying this work will be shared on reasonable request to the corresponding author.

REFERENCES

Appl S., Camenzind M., 1992, A&A, 256, 354
Begelman M. C., Blandford R. D., Rees M. J., 1984, Rev. Mod. Phys., 56, 255
Beskin V. S., 1997, Physics Uspekhi, 40, 659
Beskin V. S., 2010, MHD flows in Compact Astrophysical Objects. Springer, Heidelberg
Beskin V. S., Kuznetsova I. V., 2000, Nuovo Cimento B Serie, 115, 795
Beskin V. S., Malyshkin L. M., 2000, Astronom. Lett., 26, 208
Beskin V. S., Nokhrina E. E., 2006, MNRAS, 367, 375
Beskin V. S., Nokhrina E. E., 2009, MNRAS, 397, 1486
Beskin V. S., Pariev V. I., 1993, Phys. Uspekhi, 36, 529
Beskin V. S., Istomin Y. N., Parev V. I., 1992, Soviet Ast., 36, 642
Beskin V., Chernoglazov A., Kiselev A., Nokhrina E., 2017, MNRAS, 472, 3971
Blandford R., 1976, MNRAS, 176, 465
Blandford R. D., Payne D. G., 1982, MNRAS, 199, 883
Bogovalov S. V., 1992, Sov. Astron. Lett., 18, 337
Bogovalov S. V., 1995, Astron. Lett., 21, 565
Bogovalov S. V., 1998, Astronom Lett., 24, 321
Bogovalov S., Tsinganos K., 1999, MNRAS, 305, 211
Bromberg O., Tchekhovskoy A., 2016, MNRAS, 456, 1739
Camenzind M., 1986, A&A, 162, 32
Camenzind M., 1990, Rev. Mod. Astron., 3, 234
Camenzind M., 2007, Compact objects in astrophysics: white dwarfs, neutron stars, and black holes. Springer, Heidelberg
Chatterjee K., Liska M., Tchekhovskoy A., Markoff S. B., 2019, MNRAS, 490, 2200
Chernoglazov A. V., Beskin V. S., Pariev V. I., 2019, MNRAS, 488, 224
Chiueh T., Li Z.-Y., Begelman M. C., 1991, ApJ, 377, 462

Crinquand B., Cerutti B., Philippov A., Parfrey K., Dubus G., 2020, Phys. Rev. Lett., 124, 145101

Davis S. W., Tchekhovskoy A., 2020, ARA&A, 58, 407

Eichler D., 1993, ApJ, 419, 111

Gabuzda D. C., Murray É., Cronin P., 2004, MNRAS, 351, L89

Heyvaerts J., 1996, in Chiuderi C., Einaudi G.eds., Plasma Astrophysics. Springer, Berlin

Heyvaerts J., Norman C., 1989, ApJ, 347, 1055

Hirotani K., Okamoto I., 1998, ApJ, 497, 563

Hodge M. A., Lister M. L., Aller M. F., Aller H. D., Kovalev Y. Y., Pushkarev A. B., Savolainen T., 2018, ApJ, 862, 151

Hovatta T., Lister M. L., Aller M. F., Aller H. D., Homan D. C., Kovalev Y. Y., Pushkarev A. B., Savolainen T., 2012, AJ, 144, 105

Komissarov S., Porth O., 2021, New A Rev., 92, 101610

Komissarov S. S., Barkov M. V., Vlahakis N., Königl A., 2007, MNRAS, 380, 51

Kovalev Y. Y., Lister M. L., Homan D. C., Kellermann K. I., 2007, ApJL, 668, L27

Krolik J. H., 1999, Active galactic nuclei: from the central black hole to the galactic environment. Princeton University Press, Princeton

Lery T., Heyvaerts J., Appl S., Norman C. A., 1999, A&A, 347, 1055

Lister M. L. et al., 2016, AJ, 152, 12

Lovelace R., 1976, Nature, 262, 649

Lyubarskii Y. E., 1997, MNRAS, 285, 604

Lyubarsky Y., 2009, ApJ, 698, 1570

McKinney J. C., 2006, MNRAS, 368, 1561

McKinney J. C., Tchekhovskoy A., Blandford R. D., 2012, MNRAS, 423, 3083

Meier D. L., 2012, Black Hole Astrophysics: The Engine Paradigm. Springer, Heidelberg

Mertens F., Lobanov A. P., Walker R. C., Hardee P. E., 2016, A&A, 595, A54

Park J. et al., 2019, ApJ, 887, 147

Pelletier G., Pudritz R. E., 1992, ApJ, 394, 117

Porth O., Fendt C., Meliani Z., Vaidya B., 2011, ApJ, 737, 42

Porth O. et al., 2019, ApJS, 243, 26

Ptitsyna K., Neronov A., 2016, A&A, 593, A8

Pu H.-Y., Takahashi M., 2020, ApJ, 892, 37

Romanova M. M., Ustyugova G. V., Koldoba A. V., Lovelace R. V. E., 2009, MNRAS, 399, 1802

Takahashi M., Nitta S., Tatematsu Y., Tomimatsu A., 1990, ApJ, 363, 206

Takahashi K., Toma K., Kino M., Nakamura M., Hada K., 2018, ApJ, 868, 82

Takahashi M., Kino M., Pu H.-Y., 2021, Phys. Rev. D, 104, 103004

Tchekhovskoy A., McKinney J. C., Narayan R., 2008, MNRAS, 388, 551

Thorne K. S., Price R. H., MacDonald D. A., 1986, in, Thorne K. S., Price R. H., Macdonald D. A.eds., Black holes: The membrane paradigm. Yale University Press, New Haven

Tsinganos K., Bogovalov S., 2002, MNRAS, 337, 553

Urry C. M., Padovani P., 1995, PASP, 107, 803

Ustyugova G. V., Koldoba A. V., Romanova M. M., Chechetkin V. M., Lovelace R. V. E., 1995, ApJ, 439, L39

Ustyugova G. V., Koldoba A. V., Romanova M. M., Chechetkin V. M., Lovelace R. V. E., 1999, ApJ, 516, 221

Zobnina D. I. et al., 2022, MNRAS, 523, 3615

This paper has been typeset from a TEX/LATEX file prepared by the author.